Title:

Electrochemical Reduction Behavior of Borosilicate Glass in Molten $CaCl_2$

Authors:

Yumi KATASHO,[a] Xiao YANG, [a] Kouji YASUDA,[b,c,*] Toshiyuki NOHIRA,[a,*,z]

Affiliation:

[a]Institute of Advanced Energy, Kyoto University, Gokasho, Uji, Kyoto 611-0011, Japan.

[b]Environment, Safety and Health Organization, Kyoto University, Yoshida-hommachi, Sakyo-ku, Kyoto 606-8501, Japan.

[c]Department of Fundamental Energy Science, Graduate School of Energy Science, Kyoto University, Yoshida-hommachi, Sakyo-ku, Kyoto 606-8501, Japan.

*Electrochemistry Society Active Member

[z]**Corresponding Author:**

nohira.toshiyuki.8r@kyoto-u.ac.jp (T. Nohira)

Tel.: + 81-774-38-3500; Fax: + 81-774-38-3499.

Abstract

The electrochemical reduction behavior of borosilicate glass, which is the main component of vitrified radioactive waste, was investigated in molten $CaCl_2$ at 1123 K to establish a new nuclear waste disposal procedure. Cyclic voltammetry of borosilicate and silica glasses suggested that the reduction of B_2O_3 in borosilicate glass occurred at a more positive potential than that of SiO_2. X-ray photoelectron spectroscopy confirmed that the B_2O_3 component was reduced to B or a B-Si compound at 0.9 V vs. Ca^{2+}/Ca. The reduction products prepared by the potentiostatic electrolysis of borosilicate glass at 0.9 V had granular morphology and consisted of crystalline Si. The Al_2O_3 component was not reduced at 0.9 V and the Na_2O component was suggested to be dissolved in molten $CaCl_2$ during electrolysis.

Keywords:

Molten salt; vitrified radioactive wastes; electrochemical reduction; borosilicate glass

1. Introduction

Nuclear power was responsible for generating more than 11% of the world's electricity in 2015.[1] Since the life-cycle of greenhouse gas emissions from nuclear power is much lower than that of other conventional base load energy sources,[1] nuclear power has the potential to mitigate global warming by replacing fossil fuels in power generation.

On the other hand, nuclear power generation has challenges, particularly in the disposal of radioactive wastes. Currently, high-level nuclear wastes are confined in borosilicate glass to prepare them for ultimate disposal, *i.e.*, they are isolated until they lose enough radioactivity in a process called deep geological disposal. A typical composition of the vitrified waste is 43-53 wt% SiO_2, 7-17 wt% B_2O_3, 3-5 wt% Al_2O_3, 6-24 wt% Na_2O, and ≦25-35 wt% nuclear wastes.[2] By 2000, the vitrification facilities of the French company COGEMA (presently Areva) had produced over 10,000 canisters containing about 4,000 tons of vitrified high-level waste.[3] Globally, a significant amount of radioactive wastes have been produced in the past and even larger amounts will be produced in the future. The International Atomic Energy Agency (IAEA) reported that the total amount of spent fuel generated worldwide was about 276,000 tHM (tons of heavy metal) at the end of 2004.[4] Among them, 90,000 tHM had been reprocessed and 186,000 tHM were being stored for reprocessing.[4] However, in many countries including Japan, the places for ultimate disposal have not been determined yet. Among the difficulties in earthquake prone nations like Japan is finding stable geological layers.

To address this situation, a new disposal process has been proposed in Japan: Long-lived fission products (LLFPs) such as ^{135}Cs, ^{79}Se, ^{93}Zr, and ^{107}Pd, whose half-lives are 2.3 million, 327 thousand, 1.53 million, and 6.5 million years, respectively, in the high-level nuclear waste are separated and converted into short-lived or stable

nuclides by nuclear transmutation.[5] Since the amount of radioactive wastes is significantly decreased, the need to prepare ultimate disposal locations is eliminated. Moreover, some elements found in the waste, e.g., platinum group metals, are expected to be utilized for various applications such as automobile catalysts and fuel cell catalysts.

The LLFPs in vitrified wastes must first be recovered and then separated from each other before the transmutation process. Since the vitrified wastes are originally prepared to confine the LLFPs stably for a long time, the recovery of the LLFPs is challenging. First, a pretreatment process that can destroy the glass structure of the vitrified wastes is required. While glass can be dissolved by hydrofluoric acid, wet processes using hydrofluoric acid cannot be used in pretreatment without producing a large amount of secondary radioactive waste. In contrast, dry processes, although not studied so far, have the potential advantages of decreasing the amount of secondary wastes and providing a high processing rate. Among several conceivable dry processes, electrochemical reduction in molten salt is worth investigating because electrochemical reductions of solid metal oxides including SiO_2 in molten salts have already been established.[6,7] Furthermore, the behaviors of many fission products (FPs) in molten salts have been widely studied in the field of nuclear fuel reprocessing. Thus, it is possible to design a separation process for LLFPs in molten salts that follows a pretreatment process relying on electrochemical reduction.

To this day, many studies have been conducted on the electrochemical reduction of solid metal oxides in $CaCl_2$-based molten salts for the development of new production processes for valuable materials.[6,7] Chen et al.[8] firstly reported the direct electrochemical reduction of TiO_2 to Ti in molten $CaCl_2$. After their report, electrochemical reduction of various ionic metal oxides have been studied in molten salts on a laboratory scale (e.g. Ti[8], Cr[9], Ce[10], Nb[11], Ta[12], W[13], Ni[14], Zr[15], Dy[16], U[17]).

In addition to ionic oxides, electrochemical reduction of covalent oxide SiO_2 in molten $CaCl_2$ was also reported.[18] Since SiO_2 is an insulating material even at high temperatures, the reduction requires a special structure of electrodes called "contacting electrode". The SiO_2 contacting electrode is prepared by direct contact of the conducting material, typically a molybdenum wire, to an SiO_2 plate.[18] The reduction starts at the three-phase zone consisting of an oxide, a conductor, and a molten salt. The reaction zone spreads throughout the SiO_2 because the produced silicon has a high electric conductivity at high temperatures that generates additional electron pathways accompanied by a penetration of the molten salt into the porous Si layer.[19]

$$\text{Cathode: } SiO_2\,(s) + 4e^- \rightarrow Si\,(s) + 2O^{2-} \quad (1)$$

$$\text{Anode : } C\,(s) + xO^{2-} \rightarrow CO_x\,(g) + 2xe^- \quad (2)$$

Our group and other groups have proposed to apply the above reactions for the production of solar grade silicon,[19–38] the preparation of silicon nanowires,[25,39,40] and the preparation of negative electrode material for lithium ion batteries.[41] In these electrochemical methods, $CaCl_2$-based molten salts have been typically used as the electrolytic bath because of their high solubility of O^{2-} ions.[42]

The current state of the research concerning direct electrolytic reduction of other oxide components typically found in vitrified wastes is outlined below. For the second largest waste component – B_2O_3 – the direct electrochemical reduction in molten salts has not been reported. Incidentally, the production of elemental boron by molten salt electrolysis has been studied for almost one century. B(III) ions prepared by the dissolution of B_2O_3 have been reduced to elemental boron in a single step in KF, KCl, KCl-KF, NaCl-KCl, and NaCl-KCl-NaF molten salts.[43] Also for alkali oxides such as Na_2O, no direct electrochemical reduction study has been reported. With respect to Al_2O_3, Yan and Fray investigated the electrochemical reduction behavior in $CaCl_2$-

based molten salts and reported potential-pO^{2-} diagrams.[45] As previously reported, Al-rich Al-Ca alloys have been obtained with calcium aluminates as intermediate reduction products.

In this study, we investigated the electrochemical reduction of borosilicate glass in molten $CaCl_2$ with the aim of developing a new pretreatment method for the vitrified radioactive wastes. Since the reduction behavior of the actual vitrified radioactive wastes is expected to be complicated, borosilicate glass was selected as the study object. Specifically, Pyrex® glass was chosen from among the many kinds of borosilicate glass because it is the most typical one. The electrochemical behavior of Pyrex® glass was studied by cyclic voltammetry and the results were compared to those of SiO_2. Here, glass-seal electrodes,[24,30,39,44] which give good reproducibility for the geometry of the glass/conductor/$CaCl_2$ three-phase zone, were employed. Potentiostatic electrolysis was conducted at several selected potentials to prepare the samples for instrumental analysis. Based on these results, the electrochemical reduction behavior of borosilicate glass was determined.

2. Experimental

Figure 1 shows a schematic of the experimental apparatus. 500 g of $CaCl_2$ (> 95.0 %, Wako Pure Chemical Industries, Ltd.) crushed in a mortar was placed in an alumina crucible (outer diameter: 90 mm, height: 140 mm, purity 99%, As One Corp.) and put in an open dry chamber (HRW-60AR, Daikin Co. Ltd.). Then, the $CaCl_2$ was dried at 453 K in a vacuumed oven for more than 72 h, transferred to a quartz glass vessel, and vacuumed at 773 K for 24 h to further remove moisture. The subsequent electrochemical experiments were conducted inside the quartz glass vessel at 1123 K under a dry Ar atmosphere.

Electrochemical measurements and potentiostatic electrolysis were conducted with a three-electrode method using an electrochemical measurement system (HZ-3000, Hokuto Denko Corp.). Glass-seal electrodes (Fig. 2a) and wire-wound electrodes (Fig. 2b) were used as the working electrodes. In the glass-seal electrodes, a tungsten rod (> 99.95%, diameter: 2.0 mm, Nilaco corp.) was sealed in a borosilicate glass tube (Pyrex®, SiO_2 80.8 wt%, B_2O_3 12.5 wt%, Al_2O_3 2.3 wt%, Na_2O 4.0 wt%, K_2O 0.4 wt%, o.d. 8 mm) or a silica (SiO_2) glass tube (o.d. 6 mm). In the wire-wound electrodes, a borosilicate glass plate (Tempex®, SiO_2 81 wt%, B_2O_3 13 wt%, Al_2O_3 2 wt%, Na_2O 3.3 wt%, K_2O 0.7 wt%, 5 mm × 15 mm × 1.1 mm) or a silica glass plate (5 mm × 15 mm × 1 mm) was wound by a Mo wire (diam. 0.2 mm, > 99.95%, Nilaco Corp.).[37] The counter electrode was a graphite square rod (4 mm × 4 mm × 50 mm) and the reference electrode was an Ag^+/Ag electrode.[36] All potentials in the present paper have been calibrated by the redox potential of Ca, which was obtained by electrodepositing calcium metal on a Mo wire electrode (diam.1mm). A chromel-alumel thermocouple inserted in an alumina tube was used for the temperature control.

Following potentiostatic electrolysis, the glass-sealed electrodes were rinsed with distilled water to remove residual salts, dried at room temperature, and cut by a diamond cutter into ~5 mm long sections. The prepared samples were evaluated using an optical digital microscope (Dino Lite PRO Polarizer DILITE30 AM-413ZT, Sanko Co., Ltd.) and a scanning electron microscope (SEM; VE-8800, Keyence Corp.). They were also characterized by energy dispersive X-ray spectroscopy (EDX; EDAX Genesis APEX2, AMETEK Co. Ltd.), X-ray diffractometry (XRD; Ultima IV, Cu-Kα line, Rigaku Corp.), and X-ray photoelectron spectroscopy (XPS, JPS-9010MC, JEOL Ltd.). For the XPS measurement, potentiostatic electrolysis was conducted at 0.9 V vs. Ca^{2+}/Ca for 60 minutes, and the samples were rinsed with distilled water, 8 % HCl

aqueous solution, and 10 % NaOH aqueous solution. The powdery products recovered from the reduced glass-sealed electrodes were fixed evenly on carbon tape and then etched by Ar ion irradiation to remove the natural oxide from the surface. The spectra were calibrated by the C *1s* peak at 284.8 eV for the reduced sample and by the Si-O peak at 103.3 eV for the unreduced sample.

3. Results and Discussion

3.1 Thermodynamic calculations

Prior to the experiments, the reactions were estimated by Ellingham diagrams for oxides and chlorides. Figure 3(a) shows the Ellingham diagram for the oxides in the reaction system (MO_x, M=Si, B, Al, Na, K, and Ca). Among the components of borosilicate glass, K_2O, Na_2O, and B_2O_3 are less stable than SiO_2. These oxides are expected to be reduced at more positive potentials than the reduction potential of SiO_2 (1.25 V[37]). On the other hand, the diagram shows that the reduction of Al_2O_3 proceeds at a more negative potential. In the case of pure Al_2O_3, the formation of calcium aluminate depended on the conditions.[45] Moreover, there is a possibility of the formation of complex oxides such as $CaSiO_3$ and CaB_2O_4. Since the stability of these oxides in molten $CaCl_2$ depends on the concentration of O^{2-} ion, the construction of E–pO^{2-} diagram for boron is also required for the detailed discussion in the same manner with the reduction of SiO_2.[36] The construction of E–pO^{2-} diagrams will be reported in a separate full paper.

Figure 3(b) shows the Ellingham diagram for the related chlorides (MCl_x, M=Si, B, Al, Na, K, and Ca).[46] While the Gibbs formation energies for Na_2O and K_2O are far more positive than that of CaO, those for NaCl and KCl are as negative as that for $CaCl_2$. Thus, as outlined below by Equations 3 and 4, the reaction of Na_2O or K_2O with molten $CaCl_2$ is thermodynamically favorable.

$$Na_2O\ (s) + CaCl_2\ (l) = CaO\ (s) + 2\ NaCl\ (l) \quad (3)$$

$$\Delta G^{o}_{1123K} = -246.5\ kJ\ mol^{-1}\ (Ref.\ 46)$$

$$K_2O\ (s) + CaCl_2\ (l) = CaO\ (s) + 2\ KCl\ (l) \quad (4)$$

$$\Delta G^{o}_{1123K} = -347.7\ kJ\ mol^{-1}\ (Ref.\ 46)$$

Namely, the components of Na_2O and K_2O in the glass are expected to dissolve to molten salt as NaCl and KCl. On the contrary, for SiO_2, B_2O_3, and Al_2O_3, the reactions with molten $CaCl_2$ are unfavorable, as seen below in Equations 5-7.

$$SiO_2\ (s) + 2\ CaCl_2\ (l) = 2\ CaO\ (s) + SiCl_4\ (g) \quad (5)$$

$$\Delta G^{o}_{1123K} = 409.5\ kJ\ mol^{-1}\ (Ref.\ 46)$$

$$B_2O_3\ (l) + 3\ CaCl_2\ (l) = 3\ CaO\ (s) + 2\ BCl_3\ (g) \quad (6)$$

$$\Delta G^{o}_{1123K} = 623.2\ kJ\ mol^{-1}\ (Ref.\ 46)$$

$$Al_2O_3\ (s) + 3\ CaCl_2\ (l) = 3\ CaO\ (s) + 2\ AlCl_3\ (g) \quad (7)$$

$$\Delta G^{o}_{1123K} = 666.2\ kJ\ mol^{-1}\ (Ref.\ 46)$$

3.2 Cyclic voltammetry

Fig. 4 (a) and (b) show the cyclic voltammograms for sealed borosilicate glass and silica glass electrodes in molten $CaCl_2$ at 1123 K, respectively. The voltammograms were recorded for five consecutive cycles. The apparent current density is expressed with respect to the bottom area (the exposed area) of the tungsten rod. In the voltammogram for borosilicate glass (Fig. 4 (a)), a small cathodic current is observed from 1.8 V vs. Ca^{2+}/Ca. Since the potential is more positive than the SiO_2 reduction potential (Fig. 4(b)), this cathodic current is interpreted as the reduction of some oxides that are less stable than SiO_2. A larger cathodic current flows from 1.3 V, which corresponds to the reduction of SiO_2 to Si.[37] Moreover, a sharp increase of

cathodic current at 0.5 V is explained by the formation of Si-Ca alloys.[28, 37] After the reversal of scan direction to positive, an anodic current peak is observed at 0.7 V, which corresponds to the dissolution of Ca from Si-Ca alloys. Then, anodic current rising from 1.3 V is regarded as the reoxidation of Si to SiO_2. Finally, a small anodic current is observed from 1.8 V. This current is the reoxidation of reduction product which has been produced in the negative scan.

In both cyclic volrammograms for borosilicate and silica glass, the currents increase as the cycles are repeated. For pure SiO_2, this behavior has been explained by the increase of the reaction zone due to the formation of conductive Si from insulating SiO_2.[19] A similar mechanism is possible for the reduction of borosilicate glass.

3.3 Potentiostatic electrolysis

To confirm the reduction reaction results, potentiostatic electrolysis was conducted using borosilicate glass-sealed electrodes at 0.6 V (B-1), 0.9 V (B-2), and 1.4 V (B-3), and silica glass-sealed electrodes at 0.6 V (S-1), 0.9 V (S-2), and 1.4 V (S-3) for 30 minutes in molten $CaCl_2$ at 1123 K. Figure 5 shows current-time curves during the potentiostatic electrolysis and Figure 6 shows the microscope images of the reduced glass-sealed electrodes. In the electrolysis at 0.9 V and 0.6 V, the reduction currents for borosilicate glass are larger than those for silica glass. In addition, the current oscillations suggest the periodic change of three phase zone, which might have occurred by the generation of H_2 by reduction of hydroxyl groups in the glass. On the other hand, in Fig. 6(a), the reduced area looks smaller for borosilicate glass compared to that of silica glass. This outcome is confirmed by Fig. 6(b), where the surface reduction progressed to the side of the tube in the case of silica glass at 0.6 V. These results indicate the smaller surface reaction rate for borosilicate glass. The observed larger current and slower surface reaction for borosilicate glass are

explained by its faster inner direction progress As shown in the cross-sectional image for sample B-2 (Fig. 6(c)), the depth of the reduced portion for borosilicate glass is almost the same length as the reduced portion on the surface. At 1.4 V, the observed current is larger for borosilicate glass compared to that of silica glass, which is consistent with the cyclic voltammetry results. However, the current value is much smaller compared to the electrolysis at more negative potentials. Since noticeable change is not observed in the microscope images, the reduction did not proceed in bulk for either borosilicate glass or silica glass.

3.4 Characterization of the products

Figure 7 shows the XRD patterns for the reduced (a) borosilicate glass plate and (b) silica glass plate at 0.9 V in molten $CaCl_2$ at 1123 K. The formation of crystalline silicon was confirmed for both samples. Considering the full widths at half maximum for the peaks in two patterns, the crystallinity of produced silicon obtained from borosilicate glass was lower than that from silica glass.

Figure 8 shows XPS spectra for (a) B *1s* and (b) Si *2p* before and after the reduction of borosilicate samples. In Fig. 8 (a), a weakened B-O peak and a strengthened B-B or B-Si peak are observed for the reduced sample, which confirm the reduction of boron oxide to its metallic state. In the same manner, the reduction of silicon oxide to its metallic state is confirmed in Fig. 8(b), agreeing with the XRD analysis.

Figure 9 shows (a) a SEM image of the unreduced borosilicate glass, (b) SEM image and EDX mapping results for the reduction products obtained by the electrolysis at 0.9 V for 30 minutes, and (c) the EDX analysis results for the two specified points in the figure. Following electrolytic reduction, the flat morphology of the original borosilicate glass changes to a granular one with a diameter of 1~10 μm.

The different morphology from the previously reported result for silica glass, in which Si wires or Si columns with a diameter ~1 μm were observed[18, 19], might be attributed to the presence of boron oxide and aluminum oxide. As shown from EDX mapping results, the areas with high O concentration always contain Al, Ca, and Cl, suggesting that aluminum oxide is not reduced at 0.9 V, and that calcium aluminate forms via the reaction with CaO in the molten salt. This explanation is consistent with the potential-pO^{2-} diagram for the Al-Ca-O-Cl system.[45] Here, the detected Cl is likely due to the complex compounds with calcium aluminate and $CaCl_2$. As for Na content, the dissolution of Na_2O into molten $CaCl_2$ is suggested because the Na concentration largely decreased both in the reduced area (point 1) and unreduced area (point 2) relative to the original value. Incidentally, the concentration of K in the original borosilicate glass was below the detection limit of EDX. Considering the thermodynamic calculation and the chemical similarity with Na, the behavior of K is believed to be the same as that of Na.

4. Conclusions

The electrochemical reduction behavior of borosilicate glass, whose components were 80.8 wt% SiO_2, 12.5 wt% B_2O_3, 2.3 wt% Al_2O_3, 4.0 wt% Na_2O, and 0.4 wt% K_2O, was investigated in molten $CaCl_2$ at 1123 K. Based on cyclic voltammogram comparisons between borosilicate and silica glasses, the reduction of oxides other than SiO_2 was determined for borosilicate glass. From the Ellingham diagrams for oxides and chlorides, B_2O_3 was expected to be reduced at a more positive potential than SiO_2. In the potentiostatic electrolysis at 0.6 V (vs. Ca^{2+}/Ca) and 0.9 V, the reduction currents were larger for borosilicate glass compared to those of silica glass. The larger currents were explained by the faster reaction toward the inner glass, though the reduction rate in the surface direction was smaller than that of silica glass.

The reduction of SiO_2 to crystalline Si and the reduction of B_2O_3 to B or B-Si compound were confirmed by XRD and XPS analyses. The granular morphology with 1~10 μm diameter was observed in the reduced area by SEM and the main component of granules was Si. According to the EDX analysis, Al_2O_3 was not reduced and calcium aluminate was formed. The EDX results suggested that the Na_2O component dissolved into the molten salt during electrolysis. The behavior of the K_2O component was considered to be the same as that of Na_2O, although the analysis could not be completed because of its low concentration.

Acknowledgments

This work was partly funded by ImPACT Program of Council for Science, Technology and Innovation (Cabinet Office, Government of Japan).

References

1. *Intergovernmental Panel on Climate Change. Working Group III Climate Change 2014: Mitigation of climate change. Annex III: Technology-specific cost and performance parameters.* http://report.mitigation2014.org/report/ipcc_wg3_ar5_annex-iii.pdf.

2. M. I. Ojovan and W. E. Lee, *Metall. Mater. Trans. A*, **42**, 837 (2011).

3. *IAEA-TECDOC-1467, Status and trends in spent fuel reprocessing.* http://www-pub.iaea.org/MTCD/publications/PDF/te_1467_web.pdf.

4. *IAEA-TECDOC-1532, Operation and Maintenance of Spent Fuel Storage and Transportation Casks/Containers* http://www-pub.iaea.org/MTCD/publications/PDF/te_1532_web.pdf.

5. *Impulsing Paradigm Change through Disruptive Technologies Program. Reduction and Resource Recycle of High Level Radioactive Wastes with Nuclear Transmutation.* http://www.jst.go.jp/impact/en/program08.html.

6. W. Xiao and D. Wang, *Chem. Soc. Rev.*, **43**, 3215 (2014).

7. A. M. Abdelkader, K. T. Kilby, A. Cox, and D. J. Fray, *Chem. Rev. (Washington, DC, U. S.)*, **113**, 2863 (2013).

8. G. Z. Chen, D. J. Fray, and T. W. Farthing, *Nature (London)*, **407**, 361 (2000).

9. C. Schwandt and D. J. Fray, Z. Naturforsch. *Z. Naturforsch., A: Phys. Sci.* , **62**, 655 (2007).

10. B. Claux, J. Serp, and J. Fouletier, *Electrochim. Acta*, **56**, 2771 (2011).

11. X. Y. Yan and D. J. Fray, *Metall. Mater. Trans. B*, **33B**, 685 (2002).

12. Q. Song, Q. Xu, X. Kang, J. Du, and Z. Xi, *J. Alloys Compd.*, **490**, 241 (2010).

13. M. Erdoğan and I. Karakaya, *Metall. Mater. Trans. B*, **41B**, 798 (2010).

14. X. Y. Yan and D. J. Fray, *Miner. Process. Extr. Metall. Rev.*, **116**, 17 (2007).

15. A. M. Abdelkader, A. Daher, R. A. Abdelkareem, and E. El-Kashif, *Metall. Mater. Trans. B*, **38B**, 35 (2007).

16. P. Kim, H. Xie, Y. Zhai, X. Zou, and X. Lang, *J. Appl. Electrochem.*, **42**, 257 (2012).

17. Y. Sakamura, M. Kurata, and T. Inoue, *J. Electrochem. Soc.*, **153**, D31 (2006).

18. T. Nohira, K. Yasuda, and Y. Ito, *Nat. Mater.*, **2**, 397 (2003).

19. K. Yasuda, T. Nohira, K. Amezawa, Y. H. Ogata, and Y. Ito, *J. Electrochem. Soc.*, **152**, D69 (2005).

20. J. Cai, X. Luo, G. M. Haarberg, O. E. Kongsteinc, and S. Wang, *J. Electrochem. Soc.*, **159**, D155 (2012).

21. S. K. Cho, F. R. F. Fan, and A. J. Bard, *Angew. Chem. Int. Ed.*, **51**, 12740 (2012).

22. J. Eimutis, A. Cox, and D. J. Fray, *Electrochim. Acta*, **68**, 123 (2012).

23. E. Ergül, İ. Karakaya, and M. Erdoğan, *J. Alloys Compd.*, **509**, 899 (2011).

24. X. Jin, P. Gao, D. Wang, X. Hu, and G. Z. Chen, *Angew. Chem. Int. Ed.*, **43**, 733 (2004).

25. Y. Nishimura, T. Nohira, K. Kobayashi, and R. Hagiwara, *J. Electrochem. Soc.*, **158**, E55 (2011).

26. T. Nohira, N. Kani, T. Tsuda, and R. Hagiwara, *ECS Trans.*, **5**, 239 (2009).

27. T. Oishi, M. Watanabe, K. Koyama, M. Tanaka, and K. Saegusa, *J. Electrochem. Soc.*, **158**, E93 (2011).

28. T. Toba, K. Yasuda, T. Nohira, X. Yang, R. Hagiwara, K. Ichitsubo, K. Masuda, and T. Homma, *Electrochemistry*, **81**, 559 (2013).

29. W. Xiao, X. Jin, and G. Z. Chen, *J. Mat. Chem. A*, **1**, 10243 (2013).

30. W. Xiao, X. Jin, Y. Deng, D. Wang, and G. Z. Chen, *J. Electroanal. Chem.*, **639**, 130 (2010).

31. W. Xiao, X. Jin, Y. Deng, D. Wang, X. Hu, and G. Z. Chen, *ChemPhysChem*, **7**, 1750 (2006).

32. W. Xiao, X. Wang, H. Yin, H. Zhu, X. Mao, and D. Wnag, *RSC Adv*., **2**, 7588 (2012).

33. X. Yang, K. Yasuda, T. Nohira, R. Hagiwara, and T. Homma, *J. Electrochem. Soc*., **161**, D3116 (2014).

34. X. Yang, K. Yasuda, T. Nohira, R. Hagiwara, and T. Homma, *Metall. Mater. Trans. B*, **45B**, 1337 (2014).

35. K. Yasuda, T. Nohira, R. Hagiwara, and Y. H. Ogata, *Electrochim. Acta*, **53**, 106 (2007).

36. K. Yasuda, T. Nohira, R. Hagiwara, and Y. H. Ogata, *J. Electrochem. Soc*., **154**, E95 (2007).

37. K. Yasuda, T. Nohira, and Y. Ito, *Phys. Chem. Solids*, **66**, 443 (2005).

38. K. Yasuda, T. Nohira, K. Kobayashi, N. Kani, T. Tsuda, and R. Hagiwara, *Energy Technol.*, **1**, 245 (2013).

39. J. Yang, S. Lu, S. Kan, X. Zhang, and J. Du, *Chem. Commun. (Cambridge, U. K.)*, 3273 (2009).

40. J. Zhao, J. Li, P. Ying, W. Zhang, L. Meng, and C. Li, *Chem. Commun. (Cambridge, U. K.)*, **49**, 4477 (2013).

41. H. Nishihara, T. Suzuki, H. Itoi, B. An, S. Iwamura, R. Berenguer, and T. Kyotani, *Nanoscale*, **6**, 10574 (2014).

42. P. D. Ferro, B. Mishra, D. L. Olson, and W. A. Averill, *Waste Manage. (Oxford, U. K.)*, **17**, 451 (1998).

43. J. Zhou and P. Bai, Asia Pac. *J. Chem. Eng.*, **10**, 325 (2015).

44. P. Gao, X. Jin, D. Wang, X. Hu, and G. Z. Chen, *J. Electroanal. Chem.*, **579**, 321 (2005).

45. X. Y. Yan and D. J. Fray, *J. Appl. Electrochem.*, **39**, 1349 (2009).

46. *NIST-JANAF Thermochemical Tables.* http://kinetics.nist.gov/janaf/.

Figures captions

Fig. 1 Schematic of the experimental apparatus. (A) Working electrode, (B) graphite counter electrode, (C) Ag^{+}/Ag reference electrode, and (D) thermocouple.

Fig. 2 Photographs of (a-1) the side view and (a-2) the cross-sectional view of a glass-seal electrode and (b) a wire-wound electrode.

Fig. 3 Ellingham diagrams for selected (a) oxides and (b) chlorides [46].

Fig. 4 Cyclic voltammograms for sealed (a) borosilicate and (b) silica glass electrodes in molten $CaCl_2$ at 1123 K. Scan rate: 100 mV s^{-1}.

Fig. 5 Current-time curves during the potentiostatic electrolysis of the sealed borosilicate glass electrodes at (B-1) 0.6 V, (B-2) 0.9 V, and (B-3) 1.4 V and the sealed silica glass electrodes at (S-1) 0.6 V and (S-2) 0.9 V vs. Ca^{2+}/Ca for 30 minutes in molten $CaCl_2$ at 1123 K.

Fig. 6 (a) Microscope images of the sealed glass electrodes following potentiostatic electrolysis at 0.6 V, 0.9 V, and 1.4 V vs. Ca^{2+}/Ca for 30 minutes in molten $CaCl_2$ at 1123 K. White circle shows the boundary between the tungsten rod and the glass. (b) A surface side view of sample S-1. (b) A cross-sectional view of sample B-2.

Fig. 7 XRD patterns for the reduced (a) borosilicate glass plate and (b) silica glass plate following electrolytic reduction at 0.9 V vs. Ca^{2+}/Ca for 30 minutes in molten $CaCl_2$ at 1123 K.

Fig. 8 XPS spectra for (a) B *1s* and (b) Si *2p* for the borosilicate glass samples before and after the electrolytic reduction at 0.9 V vs. Ca^{2+}/Ca for 60 minutes in $CaCl_2$ at 1123 K.

Fig. 9 (a) SEM image of unreduced borosilicate glass. (b) SEM image and EDX maps for Si, (Si + O), (Si + Al), (Si + Cl) and (Si + Ca) of sample B-2 reduced at 0.9 V vs. Ca^{2+}/Ca for 30 minutes in molten $CaCl_2$ at 1123 K. (c) EDX analysis result for the unreduced borosilicate glass and the reduced borosilicate glass at point 1 and 2 indicated in (b).

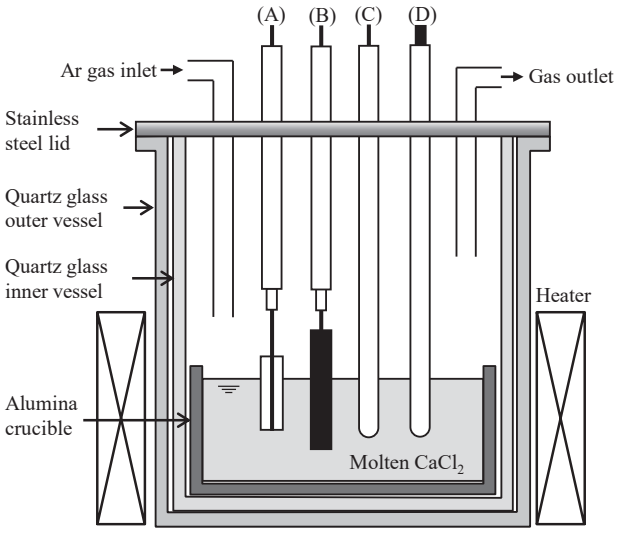

Fig. 1 Schematic of the experimental apparatus. (A) Working electrode, (B) graphite counter electrode, (C) Ag+/Ag reference electrode, and (D) thermocouple.

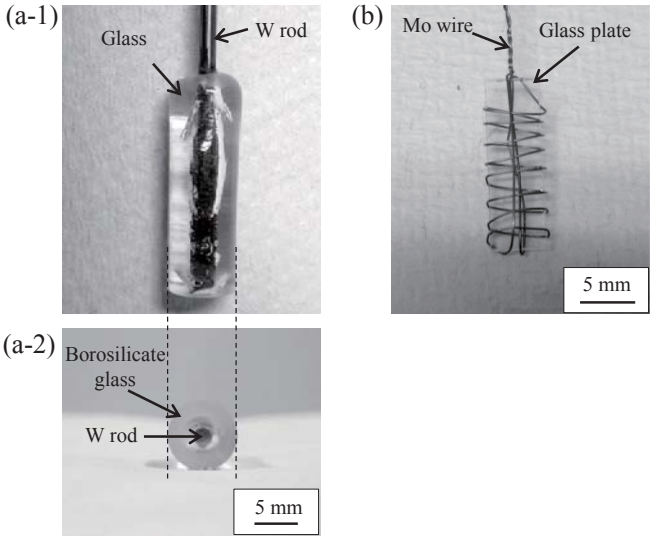

Fig. 2 Photographs of (a-1) the side view and (a-2) the cross-sectional view of a glass-seal electrode and (b) a wire-wound electrode.

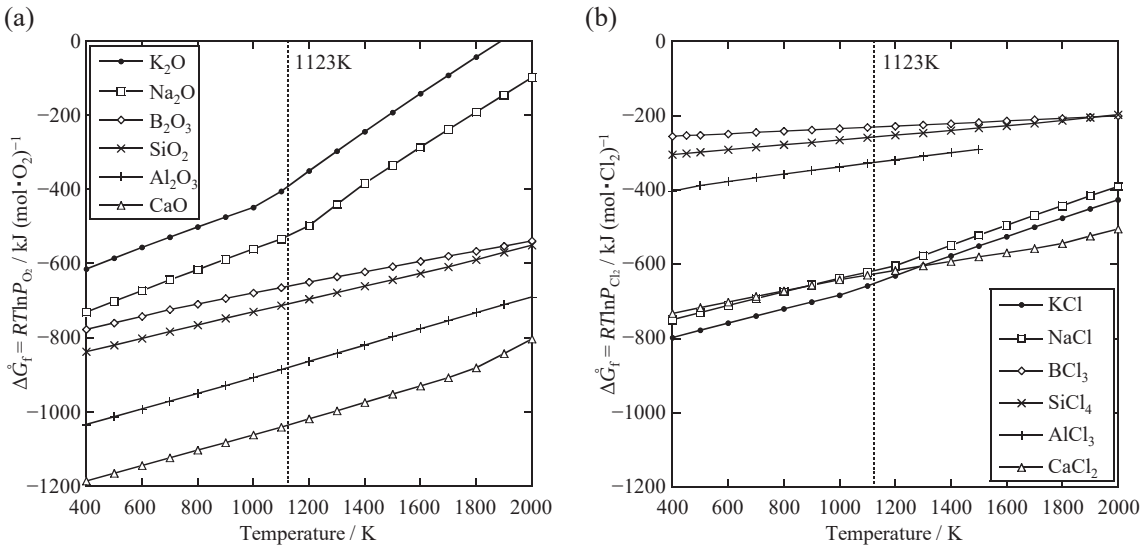

Fig. 3 Ellingham diagrams for selected (a) oxides and (b) chlorides [46].

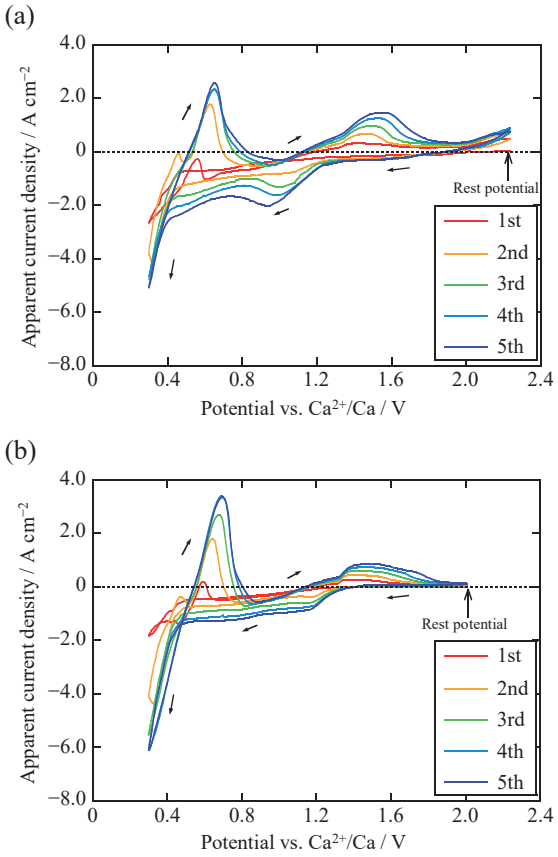

Fig. 4 Cyclic voltammograms for sealed (a) borosilicate and (b) silica glass electrodes in molten $CaCl_2$ at 1123 K. Scan rate: 100 mV s^{-1}.

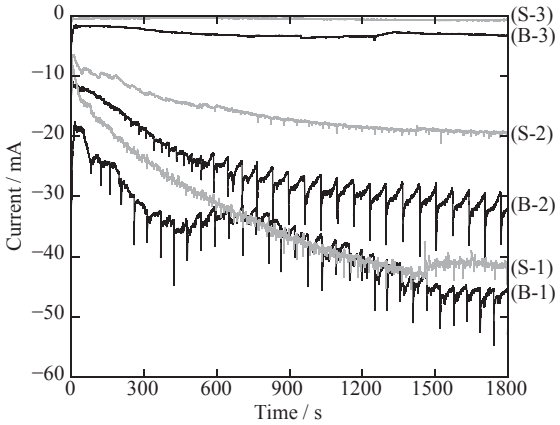

Fig. 5 Current-time curves during the potentiostatic electrolysis of the sealed borosilicate glass electrodes at (B-1) 0.6 V, (B-2) 0.9 V, and (B-3) 1.4 V and the sealed silica glass electrodes at (S-1) 0.6 V and (S-2) 0.9 V vs. Ca^{2+}/Ca for 30 minutes in molten $CaCl_2$ at 1123 K.

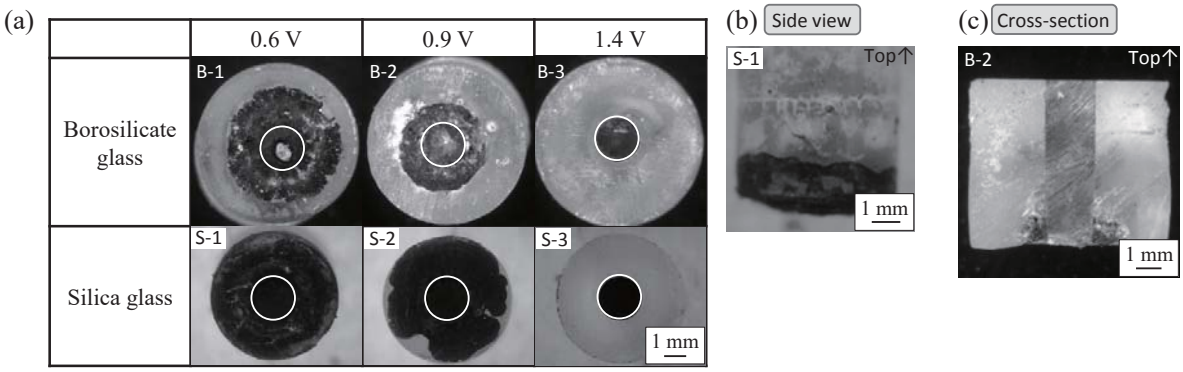

Fig. 6 (a) Microscope images of the sealed glass electrodes following potentiostatic electrolysis at 0.6 V, 0.9 V, and 1.4 V vs. Ca^{2+}/Ca for 30 minutes in molten $CaCl_2$ at 1123 K. White circle shows the boundary between the tungsten rod and the glass. (b) A surface side view of sample S-1. (b) A cross-sectional view of sample B-2.

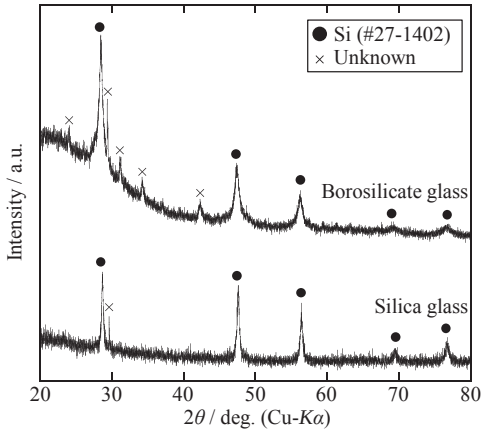

Fig. 7 XRD patterns for the reduced (a) borosilicate glass plate and (b) silica glass plate following electrolytic reduction at 0.9 V vs. Ca^{2+}/Ca for 30 minutes in molten $CaCl_2$ at 1123 K.

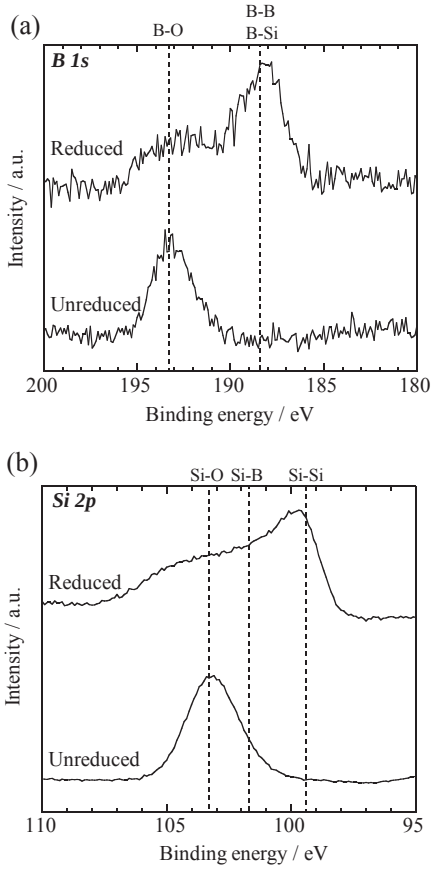

Fig. 8 XPS spectra for (a) B *1s* and (b) Si *2p* for the borosilicate glass samples before and after the electrolytic reduction at 0.9 V vs. Ca^{2+}/Ca for 60 minutes in $CaCl_2$ at 1123 K.

(a)

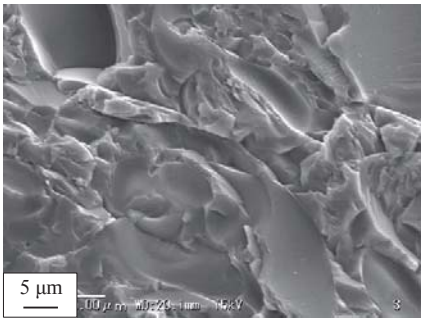

(b)

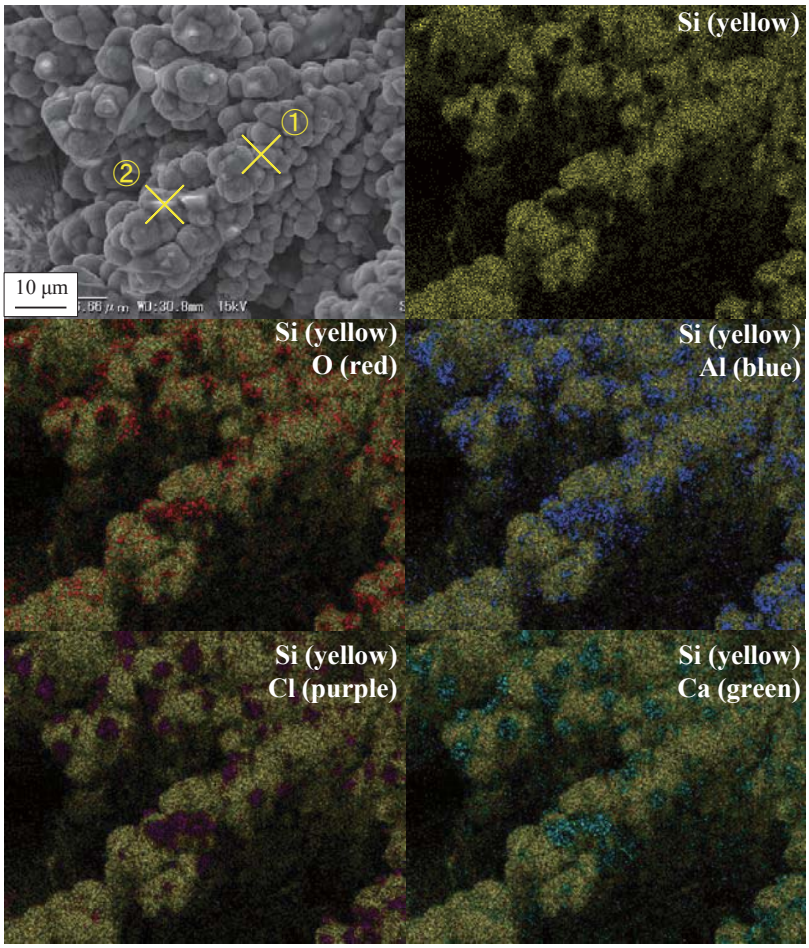

(c) (At %)

	Unreduced	①	②
Si	34.66	92.28	10.31
O	60.55	5.72	53.97
Al	1.65	1.58	11.28
Na	2.87	0.42	1.00
Ca	0.28	0.00	15.10
Cl	0.00	0.00	8.34

Fig. 9 (a) SEM image of unreduced borosilicate glass. (b) SEM image and EDX maps for Si, (Si + O), (Si + Al), (Si + Cl) and (Si + Ca) of sample B-2 reduced at 0.9 V vs. Ca^{2+}/Ca for 30 minutes in molten $CaCl_2$ at 1123 K. (c) EDX analysis result for the unreduced borosilicate glass and the reduced borosilicate glass at point 1 and 2 indicated in (b).